

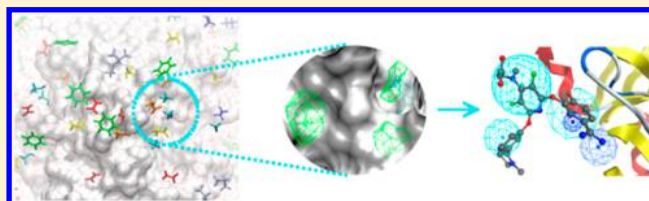
# Pharmacophore Modeling Using Site-Identification by Ligand Competitive Saturation (SILCS) with Multiple Probe Molecules

Wenbo Yu, Sirish Kaushik Lakkaraju, E. Prabhu Raman, Lei Fang, and Alexander D. MacKerell, Jr.\*

Department of Pharmaceutical Sciences, School of Pharmacy, University of Maryland, Baltimore, Maryland 21201, United States

## Supporting Information

**ABSTRACT:** Receptor-based pharmacophore modeling is an efficient computer-aided drug design technique that uses the structure of the target protein to identify novel leads. However, most methods consider protein flexibility and desolvation effects in a very approximate way, which may limit their use in practice. The Site-Identification by Ligand Competitive Saturation (SILCS) assisted pharmacophore modeling protocol (SILCS-Pharm) was introduced recently to address these issues, as SILCS naturally takes both protein flexibility and desolvation effects into account by using full molecular dynamics simulations to determine 3D maps of the functional group-affinity patterns on a target receptor. In the present work, the SILCS-Pharm protocol is extended to use a wider range of probe molecules including benzene, propane, methanol, formamide, acetaldehyde, methylammonium, acetate and water. This approach removes the previous ambiguity brought by using water as both the hydrogen-bond donor and acceptor probe molecule. The new SILCS-Pharm protocol is shown to yield improved screening results, as compared to the previous approach based on three target proteins. Further validation of the new protocol using five additional protein targets showed improved screening compared to those using common docking methods, further indicating improvements brought by the explicit inclusion of additional feature types associated with the wider collection of probe molecules in the SILCS simulations. The advantage of using complementary features and volume constraints, based on exclusion maps of the protein defined from the SILCS simulations, is presented. In addition, reranking using SILCS-based ligand grid free energies is shown to enhance the diversity of identified ligands for the majority of targets. These results suggest that the SILCS-Pharm protocol will be of utility in rational drug design.



## ■ INTRODUCTION

Pharmacophore modeling is a widely used computer-aided drug design (CADD) approach that, in addition to docking methods, is used in virtual screening (VS) studies.<sup>1,2</sup> Compared to the energy function driven docking methods, it is based on the pattern of functional groups that are crucial for interactions of ligands with the protein target. These so-called pharmacophore features, and the resulting pharmacophore models, may be used to screen against a compound database to identify ligands with functional groups that match the pharmacophore features, an approach that is often superior to ligand docking VS.<sup>3,4</sup> While pharmacophores may be developed based on the structure of known ligands, if the target protein structure is known, receptor-based pharmacophores can be constructed without knowledge of any known ligands of the target. Methods to develop receptor-based pharmacophores include the multicopy simultaneous search (MCSS) derived pharmacophore method,<sup>5</sup> the GRID molecular interaction fields (MIFs)-based method<sup>6</sup> and the recent hydration-site-restricted pharmacophore (HSRP) method.<sup>7</sup>

Although there have been a number of successes using receptor-based pharmacophore modeling,<sup>8–10</sup> the effectiveness of those methods may be limited due to neglect of protein flexibility and desolvation effects. This is due to available methods being based on only a single or limited number of

receptor conformations and being performed in vacuum or with a limited representation of the aqueous solvent environment, as discussed previously.<sup>11,12</sup> More recent works using receptor-based pharmacophore modeling methods have begun to take these concerns into account, usually by utilizing molecular dynamics (MD) simulations.<sup>13–15</sup> But effective use of information present in MD simulations to further refine pharmacophore models is still an active area of research.

The site identification by ligand competitive saturation (SILCS) approach is a method that maps the functional group requirements of proteins, including contributions from protein flexibility and desolvation. Recently, a SILCS assisted pharmacophore modeling protocol (SILCS-Pharm)<sup>16</sup> was introduced by us. The SILCS technique<sup>17</sup> naturally takes both protein flexibility and desolvation effects into account by using MD simulations in an aqueous solution that contains a collection of probe molecules. During the simulation, the probe molecules compete with water and with each other for binding sites on the protein. The binding information is then converted into probability maps of the functional group-binding patterns on the target (FragMaps) by binning the residences of probe molecule atoms into a 3D grid that encompasses the target

**Received:** November 19, 2014

**Published:** January 26, 2015

receptor. The FragMaps may then be Boltzmann transformed into a free energy representation, termed grid free energy (GFE) FragMaps, which enable its quantitative use.<sup>18</sup> Thus, the upfront calculated SILCS GFE FragMaps are an informative way to consider both protein flexibility and aqueous solvation contributions to chemical group binding that can be used for various aspects of receptor-based CADD,<sup>16–21</sup> including the context of the SILCS-Pharm method.

SILCS-Pharm converts the GFE FragMaps into pharmacophore features to enable the use of SILCS in terms of pharmacophore models. The spatial distribution of the GFE FragMaps is used to calculate feature GFEs (FGFE), which is the sum of the voxel GFEs that comprise a FragMap feature, where the voxels are based on a 3D grid that is used to define the spatial distribution of the grid free energy information in the FragMaps. The FragMap features act as the basis of the pharmacophore features and serve as a score to prioritize the identified features in an automatic fashion. Validation of the original SILCS-Pharm protocol used three representative protein targets along with ligands and decoys from the Dictionary of Useful Decoys (DUD)<sup>22</sup> with the method showing improved performance versus docking-based VS using the common docking programs DOCK<sup>23</sup> and AutoDock<sup>24</sup> and one recently developed receptor-based pharmacophore modeling technique developed by Lill and co-workers.<sup>7</sup> Although the method was shown to offer improvements over those methods, the original SILCS-Pharm protocol has limitations associated with the SILCS simulations being performed using benzene and propane as molecular probes for aromatic and aliphatic functionalities with explicit water as the probe for both hydrogen bond donors and acceptors. Thus, only four basic pharmacophore feature types are possible. In addition, there is ambiguity in differentiating between donor and acceptor FragMap features caused by the dual role played by water. Finally, using water to define the hydrogen bond donor and acceptor features disallows accounting for the energetic cost of displacing water from the associated binding sites as well as the energetic penalty associated with desolvation of the donors and acceptors upon interacting with the protein.

To overcome the above limitations, in the present work, the SILCS-Pharm protocol is extended to use the FragMaps generated using the recently extended SILCS setup.<sup>25</sup> In the extended SILCS method, besides benzene and propane, a wider range of probe molecules, including methanol, formamide, acetaldehyde, methylammonium and acetate, are used, which enables the SILCS-Pharm to cover more types of pharmacophore features. The use of explicit probe molecules for hydrogen bond donors and acceptors allows the new SILCS-Pharm protocol to generate more clearly defined hydrogen bond donor and acceptor features and avoids the ambiguity brought by the use of water as the probe for hydrogen bond interactions. Moreover, the competition between probe molecules and waters in the new SILCS protocol and the use of explicit probe molecules instead of water for donors and acceptors allows the generated pharmacophore features to take into account desolvation of both the probe molecules and the protein. The new protocol is validated using eight protein targets and associated ligands and decoys from the DUD database. Of the three protein targets that were tested using the original protocol, improvements are seen using the new SILCS-Pharm protocol. Moreover, the SILCS-based pharmacophore approach as compared to docking-based VS using DOCK 4.0, AutoDock 4 and AutoDock Vina<sup>26</sup> shows improved or

comparable results indicating its potential use in CADD. Single point and SILCS driven Monte Carlo (SILCS-MC) sampling-based ligand grid free energy (LGFE) reranking was also performed and was shown to be able to further enhance the pharmacophore modeling results, indicating the general utility of SILCS in VS.

## METHODS

**Extended SILCS-Pharm Protocol.** GFE FragMaps from SILCS simulations (see below) are used as inputs for SILCS-Pharm to build the pharmacophore features. Similar to the previous protocol,<sup>16</sup> the new SILCS-Pharm protocol contains four steps to generate a pharmacophore model: (1) voxel selection; (2) voxel clustering and FragMap feature generation; (3) FragMap feature to pharmacophore feature conversion; (4) generation of pharmacophore hypotheses (i.e., models) for VS. The first step is designed to identify crucial binding patterns from the GFE FragMaps within a specified binding region. As the GFE represents the binding strength of a functional group at a specific location on the protein surface, it allows for voxels with the most favorable interactions to be identified based on a user assigned GFE cutoff. Clustering is then performed on the selected voxels in the second step to identify interaction patterns yielding FragMap features. In the third step, the FragMap features are classified, combined and converted into SILCS pharmacophore features. Finally, all the pharmacophore features are prioritized using FGFE score, from which pharmacophore hypotheses are generated and evaluated.

Presented in Table 1 are the FragMaps types and the corresponding FragMap features. The FragMap features are

**Table 1. Correspondence between FragMap Features and Pharmacophore Features Used in SILCS-Pharm**

FragMaps and FragMap features	pharmacophore features <sup>a</sup>
APOLAR (AROM+ALIP)	AROMIALIP
HBDON	
HBACC	HBACC
POS	
NEG	NEG
AROM	AROM
ALIP	ALIP
HBDONp	HBDON
POSp	POS
MEOO	
MEOH	
FORN	

<sup>a</sup>Only basic pharmacophore features are shown here for hydrogen bond donor and acceptors; donor and acceptor joint pharmacophore features are also available as described in the text.

then converted to commonly used pharmacophore features,<sup>3,4</sup> which are also listed in Table 1. Conversion from FragMap features to pharmacophore features involves analysis to determine, for example, whether a FragMap associated with the hydrogen or oxygen of the alcohol in methanol should be assigned a hydrogen bond donor (HBDON) or acceptor (HBACC) pharmacophore feature based on the geometric criteria described below.

The considered FragMaps and corresponding FragMap features are as follows. Five generic FragMap types are considered: (1) generic nonpolar (APOLAR, benzene and propane carbons); (2) generic neutral donor (HBDON,

methanol and formamide polar hydrogens; (3) generic neutral acceptor (HBACC, methanol, formamide, and acetaldehyde oxygens); (4) positive donor (POS, polar methylammonium hydrogens); (5) negative acceptor (NEG, acetate oxygens). In addition, seven specific FragMaps are constructed: (6) aromatic (AROM, benzene carbons); (7) aliphatic (ALIP, propane carbons); (8) generic neutral hydrogen bond donor parent atoms (HBDONp, methanol oxygen and formamide nitrogen); (9) positive donor nitrogen parent atom (POSp, methylammonium nitrogen); (10) methanol oxygen atom (MEOO); (11) methanol hydrogen atom (MEOH); (12) formamide nitrogen (FORN).

Conversion of FragMaps to FragMap features in step 2 is based on a clustering algorithm. A hierarchical clustering algorithm was used previously with a user defined cluster member distance parameter to determine voxels that belong to the same cluster. A default value of 1 Å was used for hydrogen bond donor and acceptor voxel clustering because the voxel size is 1 Å × 1 Å × 1 Å, such that only neighboring voxels are included in a cluster. However, a larger distance parameter, in the range of 2.8 Å, was used for aromatic and aliphatic voxel such that the clusters included both neighboring as well as near but discrete voxels. However, as part of this study, it was found that GFE cutoffs alone can serve as the sole parameter to select neighboring voxels to define a cluster by simply setting the cluster member distance parameters to 1 Å such that only neighboring voxels define a given cluster. In cases where discrete voxels are adjacent to a cluster, they are treated as separate FragMap features.

Step 3 involves conversion of the FragMap features to pharmacophore features. First, the hydrophobic features (APOLAR, AROM and ALIP) are considered. If an APOLAR FragMap feature overlaps with both AROM and ALIP FragMap features, then an AROMALIP joint pharmacophore feature is defined. If an APOLAR FragMap feature only overlaps with AROM FragMap feature, then an AROM pharmacophore feature will be defined. Otherwise, an ALIP pharmacophore feature is defined. HBACC and NEG FragMap features are directly converted into respective HBACC and NEG pharmacophore features.

Conversion of hydrogen bond donor pharmacophore features is more complex. First, overlaps between HBDON and HBDONp FragMap features are identified. Only those HBDONp FragMap features that have overlap with HBDON features are retained, as that overlap indicates that the HBDONp is a true representative of a hydrogen bond donor. Next, MEOO and MEOH FragMap features are identified and only those MEOO FragMap features that overlap with MEOH features are retained, again as they represent true hydrogen bond donors. Finally, overlap of the remaining HBDONp FragMap features with the remaining MEOO FragMap features is identified. If the HBDONp FragMap feature overlaps with both MEOO and FORN FragMap features, then the HBDONp FragMap feature is assigned as a HBDON pharmacophore feature. Or if the HBDONp FragMap features overlap only with an FORN feature, then the FORN feature is used to define a HBDON pharmacophore feature.

Finally, it is possible that both HBACC and HBDON pharmacophore features or both charged and neutral features are found in the same location. Features at these locations are then defined as joint hydrogen bond features. The possible joint polar pharmacophore features include HBDON|POS, HBACC|NEG, HBDON|HBACC, (HBDON|POS)|HBACC,

HBDON|(HBACC|NEG) and (HBDON|POS)|(HBACC|NEG).

**SILCS Simulations and FragMap Preparation.** SILCS simulations were performed using the new SILCS setup<sup>25</sup> for the eight target proteins. FragMaps for HIV protease (HIVPR), Factor Xa (FXa) and P38MAP kinase (P38 MAP) were obtained from our previous study,<sup>25</sup> whereas FragMaps for remaining targets were calculated as part of the present study. Crystal structures were obtained from the Protein Data Bank (PDB)<sup>27</sup> for the targets Dihydrofolate reductase (DHFR, PDB ID: 3DFR), Fibroblast Growth Factor Receptor 1 kinase (FGFR1, PDB ID: 3KY2), Adenosine deaminase (ADA, PDB ID: 1NDW), Estrogen Receptor- $\alpha$  Ligand-Binding Domain (ER, PDB ID: 3ERT) and AmpC  $\beta$ -lactamase (AmpC, PDB ID: 1XGJ) and used to initialize the SILCS simulations. For holo structures, the ligands were removed while coordinated metal ions and crystal waters were retained. The Reduce software<sup>28</sup> was used to determine the optimal protonation states of histidine and side-chain orientations of asparagine and glutamine residues. GROMACS<sup>29</sup> tools were used to prepare the simulation systems involving protein, water and small probe molecules. Ten simulation systems with randomly positioned solutes at approximately 0.25 M each were simulated for 40 ns using GROMACS<sup>29</sup> with the systems being described using CHARMM22 protein force field<sup>30</sup> with CMAP backbone correction,<sup>31</sup> CHARMM General force field (CGenFF)<sup>32,33</sup> and the TIP3P water model<sup>34</sup> modified for the CHARMM force field.<sup>35</sup> For ADA, distance restraints with force constants of 1000 kJ/mol/nm<sup>2</sup> were applied between the zinc ion and the four coordinating residues during the MD simulation; analysis shows that the structure of the zinc ion and the coordinating ligands were well maintained in the simulations.

FragMaps were generated by binning selected solute atoms into voxels of a 1 Å spaced grid spanning the simulation systems. 3D normalized probability distributions were obtained by dividing the voxel occupancies computed in the presence of the protein by the respective values in bulk. The normalized distributions were Boltzmann-transformed to free energies for each FragMap type to yield GFE FragMaps. The convergence of the FragMaps was monitored by calculating overlap coefficients (OC) as previously described.<sup>25</sup> The ten trajectories for each SILCS simulation were divided into two groups as trajectories 1–5 and trajectories 6–10, and FragMaps from each group were separately computed and the OC was calculated between the two groups. As shown in the Supporting Information Table S1, all FragMaps for all the targets have OC values greater than 0.7, indicating good convergence as previously discussed.<sup>25</sup>

**Pharmacophore VS and Performance Evaluation.** VS was performed using the MOE software package.<sup>36</sup> All ligands or decoys for a target were extracted from the DUD database in mol2 format and were then converted into MOE database files. Ligand and decoy conformations were searched using the “Conformation Import” application in MOE<sup>36</sup> and up to 100 low-energy conformations defined by the MMFF94x force field<sup>37</sup> were retained for each molecule using the default MOE settings. SILCS pharmacophore models given by SILCS-Pharm were prepared in MOE pharmacophore query file format and used for VS with the default settings. The root-mean-square deviation (RMSD) between the matched features in a query molecule and the SILCS pharmacophore model was used as an activity score and the best matched conformation for each molecule with the smallest RMSD among all 100 conforma-



tions was then used as the pharmacophore predicted binding pose.

The performance of the new SILCS-Pharm protocol was compared with three other docking-based VS methods using DOCK 4.0,<sup>23</sup> AutoDock 4<sup>24</sup> and AutoDock Vina.<sup>26</sup> For the DOCK 4.0 VS, an in-house protocol, as applied in a number of CADD projects,<sup>38,39</sup> was used and the sum of electrostatic and van der Waals (vdW) energies as defined in DOCK 4.0 was used for final compound ranking. For AutoDock 4 and AutoDock Vina VS, mol2-formatted files for ligands and decoys as well as pdb-formatted files for the crystal protein structures from DUD were converted into pdbqt-formatted files to generate AutoDock atom types.<sup>24</sup> For AutoDock 4, energy grid map files with probe atoms covering all possible atom types within the database were generated and used to guide the docking search. The Lamarckian genetic algorithm (LGA)<sup>40</sup> was adopted for the docking run and 20 independent runs with a maximum of 1 750 000 energy evaluations and 27 000 GA generations were conducted. AutoDock 4 energy scores, including electrostatic, vdW and desolvation terms,<sup>40</sup> of the top 20 conformations for each molecule were averaged and the mean value was used for the final score ranking. For AutoDock Vina, the energy grid maps were calculated on-the-fly within a docking run and 20 binding modes were generated for each database molecule. The final score for each molecule used for AutoDock Vina was given by the mean score value averaged from the empirical energy scores<sup>26</sup> of the top 20 predicted binding conformations. As used in our previous study<sup>16</sup> and in the DUD paper,<sup>22</sup> enrichment plots, showing the percentage of ranked ligands at any given percentage of ranked database were employed to evaluate the VS performance. Enrichment factor (EF) reflecting the ability of a method to find more true positives while maintaining a low level of false positive rate is calculated following ranking of all the ligands and decoys, as follows

$$EF_{\text{subset}} = \frac{N_{\text{ligands\_in\_subset}}/N_{\text{ligands}}}{N_{\text{decoys\_in\_subset}}/N_{\text{decoys}}} \quad (1)$$

where subset is defined by the percentage of the ranked decoys,  $N_{\text{ligands\_in\_subset}}$ ,  $N_{\text{ligands}}$ ,  $N_{\text{decoys\_in\_subset}}$  and  $N_{\text{decoys}}$  are the number of active ligands in a subset, total number of active ligands, number of decoys in a subset and total number of decoys. EFs at 1% ( $EF_1$ ), 10% ( $EF_{10}$ ) and 20% ( $EF_{20}$ ) of the ranked decoys, which represent early and late stage enrichment performance, were calculated. The overall enrichment performance considering the whole database was also assessed by calculating the area-under-the-curve (AUC), which was evaluated from the Receiver Operating Characteristic (ROC) curve.<sup>41</sup> Similar to the previous study,<sup>16</sup> because not all molecules in the database are assigned an RMSD score in a pharmacophore VS run due to the fact that they do not have the correct number and type of features, failed ligands and decoys are ranked at the end of the ranking list with decoys ranked above ligands to allow for a direct and unbiased comparison with the docking results, where all molecules have a score and can be ranked.

**LGFE Calculation and SILCS-MC Sampling.** To test the utility of including energetic information to supplement the SILCS pharmacophores, LGFE scores,<sup>25</sup> were used to rerank the pharmacophore modeling results. The LGFE was defined using

$$LGFE = \frac{\sum GFE(i_T)}{N_C} \times N_H \quad (2)$$

where the summation is over all GFE FragMap types,  $T$ , and applicable atoms assigned to specific FragMap types,  $i_T$ .  $N_C$  is the number of GFE FragMap classified atoms and  $N_H$  is the total number of non-hydrogen heavy atoms. The FragMap assignment is based on an atom classification rule file that translates CGenFF atom types into the FragMap classes (Table S4 of the Supporting Information).

Two types of LGFE scores were used depending on whether only a single conformation or an ensemble of conformations from MC sampling were used. The single point (SP) LGFE was calculated by using the conformations directly obtained from the pharmacophore search. To allow for local conformational relaxation and generation of an ensemble of conformations, the SILCS-MC<sup>25</sup> approach was used. This uses the GFE FragMaps to drive the MC sampling and CGenFF parameters<sup>32,33</sup> to describe the intramolecular energy terms. For each compound, ten SILCS-MC runs with different random initialization seeds starting from the pharmacophore conformation were conducted for 5000 steps with small MC step sizes (molecular translation, rotation and dihedral rotation step sizes are 0.05 Å, 1 and 1 degrees) to minimize the extent that ligand would shift from the starting conformation. The LGFEs of all MC snapshots across the ten runs were Boltzmann averaged to generate the final SILCS-MC-based LGFE score. A GFE upper energy cutoff of 3 kcal/mol was used in both types of LGFE calculations, such that both favorable and unfavorable GFE FragMap contributions contribute to the LGFEs.

## RESULTS AND DISCUSSION

**SILCS Pharmacophore Models.** An in-house FORTRAN program was used for the extended SILCS-Pharm protocol to generate SILCS pharmacophore models for the eight protein targets. The choice of the GFE cutoffs, which controls the selection of voxels to be used in FragMap features for subsequent generation of the pharmacophore features, was made on a case-by-case basis. This involved visual inspection of the FragMaps at different GFE cutoffs. The GFE cutoffs were then adjusted to achieve well-separated clusters of voxels of a specific type so that the total number of resulting features within the binding region was less than 8. GFE cutoffs used for the eight targets are listed in Table S2 in the Supporting Information along with the number of features. Once the GFE cutoffs were selected, the pharmacophore features were generated as described in the methods. We note that in our previous study, the use of only water to define hydrogen bond donor and acceptor pharmacophore features required the use of detailed geometric criteria. The use of a wider range of FragMaps types greatly simplifies the assignment of pharmacophore features, with the only complications involving the identification of true hydrogen bond donor pharmacophore features.

In addition to the pharmacophore features, volume constraints associated with “forbidden regions” are considered in the final pharmacophore models. Forbidden regions are defined on the 3D grid as voxels where the SILCS solutes as well as water do not sample during the SILCS simulations (i.e., voxels with zero solute or water occupancies considering all atoms including hydrogens). Thus, instead of, for example, using the protein surface to define regions where ligands cannot be sampled during VS, an exclusion map representing the

Table 2. DUD Data Sets for the Protein Targets Used in Virtual Screening

targets	classification	DOCK 3.5 EF <sub>1</sub> <sup>a</sup>	number of ligands		number of decoys	
			all molecules	unique molecules <sup>b</sup>	all molecules	unique molecules <sup>b</sup>
HIVPR	other enzymes	3.7	62	53	2038	1885
FXa	serine proteases	14.6	146	142	5745	5095
DHFR	folate enzymes	21.7	410	201	8367	7145
FGFR1	kinases	0	120	118	4550	4205
P38 MAP	kinases	2.1	454	256	9141	8387
ADA	metalloenzymes	12.9	39	23	927	821
ERantagonist	nuclear hormone receptors	12.7	39	39	1448	1395
AmpC	other enzymes	17.1	21	21	786	732

<sup>a</sup>Published 1% enrichment factors for the DOCK 3.5 results from the DUD paper,<sup>22</sup> which can be treated as an indicator for the test case difficulty.

<sup>b</sup>In the DUD data sets, some molecules are represented in multiple forms considering different tautomer and protonation states. For the final VS result, only the most favorable scored state based on the most favorable energy score for docking and lowest RMSD for pharmacophore matching for each molecule was used.

forbidden region from the SILCS simulations is used to define a volume constraint in the pharmacophore model. This exclusion map may be considered a better alternative to more traditional representations of the protein surface since it takes the protein flexibility into account in an explicit way. Essentially, the excluded volume associated with the protein is being defined based on solute and water inaccessibility in the context of protein flexibility rather than by the space occupied by the protein in any given or all conformations.

Selection of the final SILCS pharmacophore model for screening was based on the use of the partial matching mode in VS, where the ligands only have to match a subset of “key” pharmacophore features. The key pharmacophore features are defined as those features with the most favorable FGFE scores, where the user can define the number of key features. The remaining pharmacophore features in the binding region are then defined as complementary features, which may or may not be matched in VS. Thus, during VS, only those compounds that have the correct number and types of functional groups that match the key pharmacophore features are selected. Alignment of the compounds with the key pharmacophore features as well as with complementary features if possible is then performed. Matching of complementary features in addition to the key features allows for more possible binding modes to be identified. Final RMSD scores are based on all the key and complementary features matched for a given ligand.

In summary, five advantages over the original SILCS-Pharm protocol are present in the new approach. First, charged features are introduced yielding 6 instead of 4 basic pharmacophore features. Second, with the use of explicit probes for hydrogen bond donors and acceptors instead of water, hydrogen bond donor features are more accurately described. Third, simple overlap of FragMap features are used to define the shape of joint features instead of the more complex geometric description used before. Fourth, exclusion maps are used to construct volume constraints that define the shape of the binding region, thereby including protein flexibility in the definition of the binding site shape. As shown below, the inclusion of the excluded region decreases the number of false positive hits making the SILCS pharmacophore models more specific. Last, the inclusion of all SILCS pharmacophore features in the model and the use of partial matching during pharmacophore VS is anticipated to further improve the hit rate.

**Test Set.** To test the extended SILCS-Pharm protocol, eight protein targets were selected (Table 2). All the targets have the

corresponding ligands and decoys in the DUD database.<sup>22</sup> The proteins include HIV protease (HIVPR), Factor Xa (FXa), dihydrofolate reductase (DHFR), fibroblast growth factor receptor kinase 1 (FGFR1), P38 mitogen activated protein kinase (P38 MAP), adenosine deaminase (ADA), estrogen receptor (ER) and AmpC  $\beta$ -lactamase (AmpC), and were chosen based on several considerations. HIVPR, FXa and DHFR were selected because they were used to test the previous SILCS-Pharm method, allowing for comparison with the present, extended method. The eight proteins are from different families according to the DUD classification allowing the new protocol to be tested on more target types. The numbers of active ligands and decoys vary from 21 to 256 and 732 to 8387 for the tested targets, respectively, which may help to reduce biases due to data set size effects. In addition, the selected proteins have different difficulties as reflected by the enrichment performances of docking using DOCK<sup>22</sup> with the enrichment factor varying from 0 (no enrichment) to 20 (good enrichment).

**SILCS Pharmacophore Features for the Tested Targets.** Figure 1 shows the SILCS-Pharm derived pharmacophore features together with the corresponding FragMaps contoured at the GFE cutoff levels used to generate the features. Consistent with steps 1 and 2, all FragMaps within the binding pockets have been identified as pharmacophore features and are fully covered by the pharmacophore feature spheres. Besides the basic features, various joint pharmacophore features are seen in all the targets and have been generated correctly. For example, both aromatic (in purple) and aliphatic (in green) FragMaps can be found at the same locations as the AROM|ALIP joint features colored in cyan. For DHFR (Figure 1c) both neutral (blue) and charged (iceblue) donor FragMaps can be found in a deeply buried subsite and this is represented as a HBDON|POS joint pharmacophore feature colored in yellow. For ADA (Figure 1f) both neutral hydrogen bond donor (blue) and acceptor (red) as well as charged donor (iceblue) FragMaps can be seen at the top left region, and this forms a (HBDON|POS)|HBACC feature colored in pink. In the lower left region both neutral hydrogen bond donor and acceptor features are present and result in a HBDON|HBACC feature (pink). Figure 1 also shows that the generated feature spheres can penetrate into the protein surface of the crystal structure used to initialize the SILCS simulation, indicating that protein flexibility is considered in the SILCS pharmacophore features.



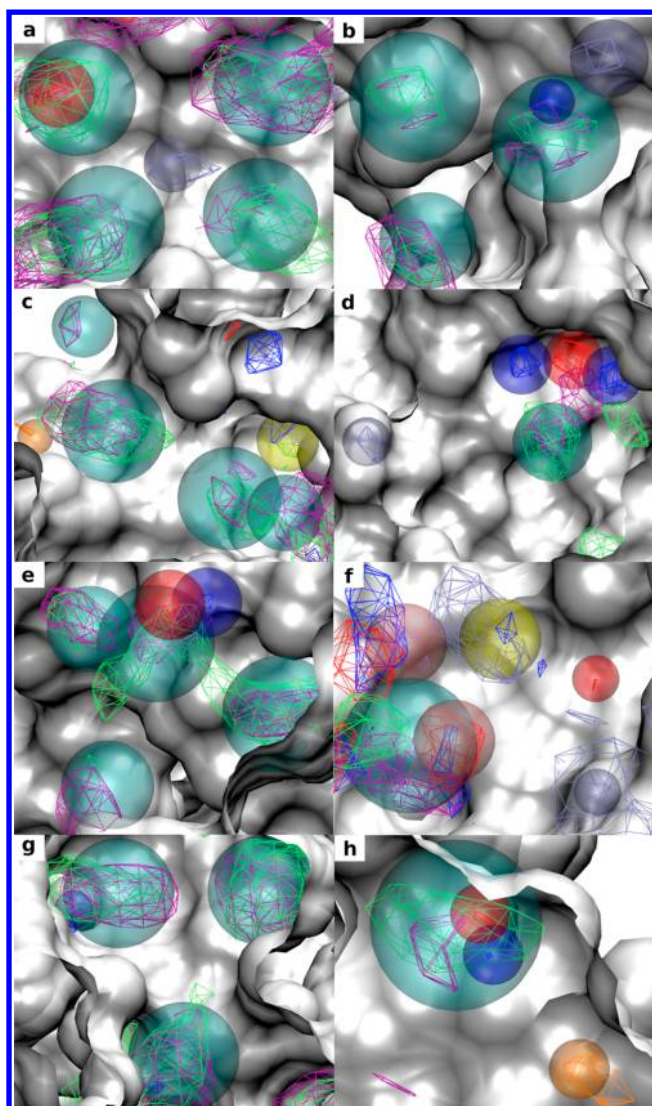


**Figure 1.** FragMaps and identified SILCS pharmacophore features within the binding pockets of the eight protein targets: (a) HIVPR (PDB ID: 1G2K); (b) FXa (PDB ID: 1FJS); (c) DHFR (PDB ID: 3DFR); (d) FGFR1 (PDB ID: 3KY2); (e) P38 MAP (PDB ID: 1OUY); (f) ADA (PDB ID: 1NDW); (g) ER (PDB ID: 3ERT); (h) AmpC (PDB ID: 1XGJ). FragMap contours are displayed at the GFE cutoffs used to generate the pharmacophore features. The color of the AROM, ALIP, HBDONp, HBACC, POSp and NEG FragMaps are purple, green, blue, red, iceblue and orange, respectively. Pharmacophore features are shown by transparent spheres. The color of the AROMIALIP, HBDON, HBACC, POS, NEG and HBDONIPOS pharmacophore features are cyan, blue, red, iceblue, orange and yellow. The joint pharmacophore feature (HBDONIPOS)HBACC (top left) and HBDONIHBACC (lower left) are colored in pink. The protein surfaces are based on the crystal structures used to initialize the SILCS simulation (white). Protein atoms occluding the view of the pocket are removed to facilitate visualization.

To more clearly analyze the importance of the inclusion of protein flexibility, we compare the SILCS exclusion maps with the surfaces of the crystal protein structures used to initialize the SILCS simulations (four targets are shown in Figure 2, and results for all targets are shown in Figure S1 in the Supporting Information). Crystal orientations of selected ligands from protein complexes other than those used for SILCS simulation are also shown for each target in the figure. Clashes are seen

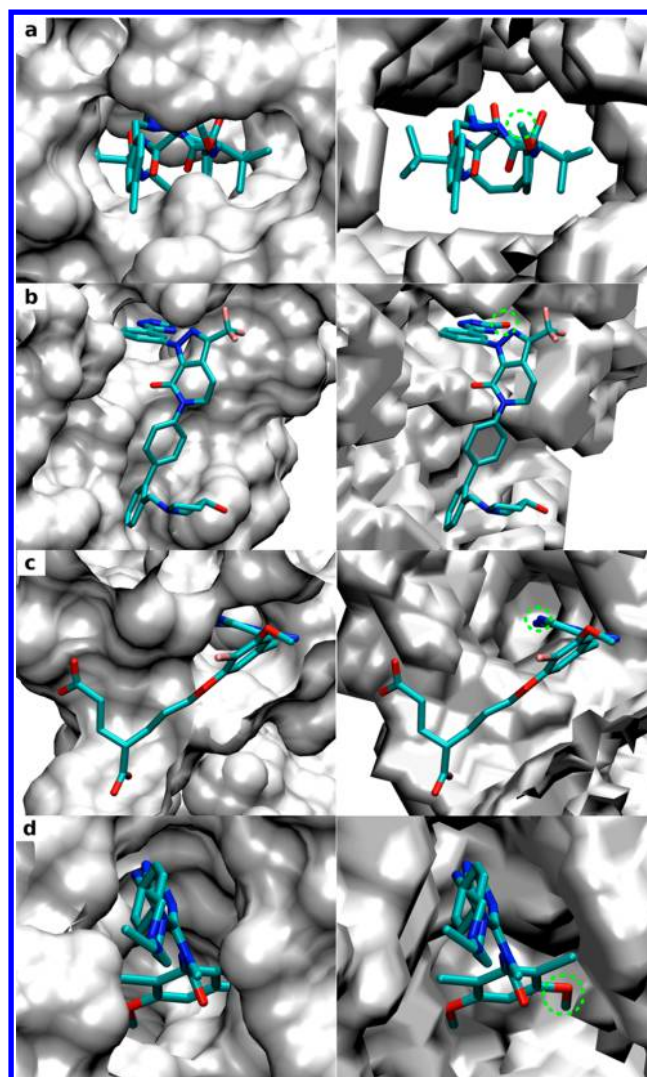


**Figure 2.** Comparison of the solvent accessible surfaces of crystal protein structures used to initialize the SILCS simulation (left panel) and SILCS exclusion maps (right panel) for the four targets: (a) HIVPR (PDB ID: 1G2K); (b) FXa (PDB ID: 1FJS); (c) DHFR (PDB ID: 3DFR); (d) FGFR1 (PDB ID: 3KY2). Results for other targets can be found in Figure S1 in the Supporting Information. The crystal binding orientation of a selected ligand for each target presents in protein–ligand complex other than the one used for SILCS simulation is also shown: (a) HIVPR (PDB ID: 3ZPS); (b) FXa (PDB ID: 3FFG); (c) DHFR (PDB ID: 1DIU); (d) FGFR1 (PDB ID: 3TT0). The green dashed circle indicates ligand atoms that have clashes with the protein surface but not the exclusion map.

between the ligand atoms with the surface of the rigid protein structure indicating that such crystal binding modes of the ligands cannot be predicted when using rigid protein structure. In contrast, the exclusion maps define a much broader binding region and the presented binding modes of the ligands are allowed indicating the importance of including protein flexibility during pharmacophore model development as well as binding mode prediction. Table 3 shows the calculated surface area (SA) for the exclusion map and crystal protein surface. The much lower SA values for the exclusion maps further indicates how additional accessible area is available when using the exclusion maps versus that using the rigid protein structure.

**Table 3.** Surface Area (SA in Å<sup>2</sup>) Calculated for the Crystal Protein Structures and Exclusion Maps of the Eight Targets

target	protein surface	exclusion map
HIVPR	20170	11440
FXa	28909	17465
DHFR	16975	8426
FGFr1	31598	15206
P38 MAP	36332	17100
ADA	35941	20066
ER	25280	10549
AmpC	35790	19826

SILCS FragMaps have been shown to recapitulate crucial ligand–protein interactions and reproduce the crystal binding modes of ligands for a number of proteins.<sup>17,18,25</sup> For the protein targets studied here, FragMaps are also found to reproduce crucial binding modes as indicated by the overlaps between the SILCS FragMap-derived pharmacophore features and functional groups in selected crystallographically identified ligands (Figure 3). Ranking of the pharmacophore features for each target based on the FGFE scores is also shown in Figure 3. Such ranking may serve as an indicator for the importance of a

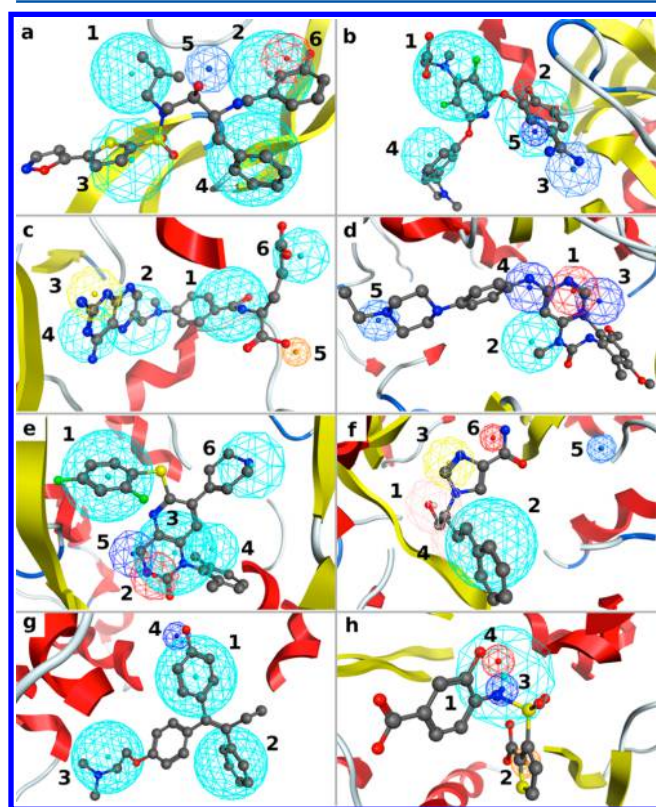


**Figure 3.** SILCS pharmacophore models for the eight protein targets with the crystal orientations of a representative ligand for each target: (a) HIVPR (PDB ID: 3SAC); (b) FXa (PDB ID: 1FJS); (c) DHFR (PDB ID: 3DFR); (d) FGFr1 (PDB ID: 3TT0); (e) P38 MAP (PDB ID: 1OUY); (f) ADA (PDB ID: 1NDW); (g) ER (PDB ID: 3ERT); (h) AmpC (PDB ID: 1XGJ). Protein atoms occluding the view of the pocket are removed to facilitate visualization. The colors of the features are the same as used in Figure 2. Numbering indicates the rank ordering of the pharmacophore features based on the FGFE scores.

feature and may potentially be used as weighting factors when doing scoring during VS.

In general, the pharmacophore features recapitulate interactions that have been shown experimentally to be important for ligand binding and FGFE can qualitatively rank the relative feature importance. For HIVPR (Figure 3a), the four hydrophobic features were the highest ranked, consistent with the fact that these four nonpolar binding pockets were known to be important for binding.<sup>42,43</sup> The fifth feature is a POS feature occupying the catalytic site where the ligand hydrogen bond donor groups, usually neutral hydroxyl groups, interact with the two Asp residues. As discussed previously,<sup>25</sup> this inconsistency is due to the Asp residues being deprotonated in the SILCS simulation, while only one Asp residue may be deprotonated.<sup>44</sup> For FXa (Figure 3b), two of the three top ranked hydrophobic features are located in the well-studied S1 and S4 pockets, which were shown to be crucial for binding of the known inhibitors,<sup>45,46</sup> and the third ranked POS feature also reproduces the commonly observed binding pattern among the known inhibitors.<sup>45</sup> For DHFR (Figure 3c), features 1, 2 and 4 reproduce the hydrophobicity of the core region in the buried binding pocket and feature 3 is a HBDONIPPOS joint feature corresponding to the surrounding charged Asp and neutral Thr residues that have both been shown to be important for ligand binding.<sup>47</sup>

For FGFr1 (Figure 3d), the three top ranked hydrogen bond donor and acceptor features 1, 3 and 4 reproduce the known binding patterns that involve critical hydrogen bond interactions with the Ala and Glu backbone carbonyl and amide groups of the hinge region at the ATP-binding pocket.<sup>48</sup> For P38 MAP, the three top ranked features 1, 2 and 3 reproduce the three functionalities that are conserved among the majority of P38 MAP inhibitors (Figure 3e).<sup>49–51</sup> The last ranked hydrophobic features 4 and 6 and neutral hydrogen bond donor feature 5 represent functional groups that are present in some, but not all inhibitors.<sup>49,50</sup> For ADA (Figure 3f), top ranked hydrophobic feature 2, hydrogen bond donor and acceptor joint features 1 and 4 all reproduce known binding interactions,<sup>52,53</sup> which involve hydrophobic residues, His17 and Asp19, respectively. For target ER (Figure 3g), the three top ranked hydrophobic features and the donor feature ranked 4th are consistent with the known binding modes of ER antagonists.<sup>54,55</sup> As seen in Figure 3h the top ranked hydrophobic feature 1 mimics the stacking interaction with Tyr221 residue<sup>56,57</sup> and the second ranked feature NEG recapitulates the oxyanion hole caused by the catalytic residue Ser64.<sup>56,57</sup> Neutral hydrogen bond donor and acceptor features 3 and 4 are related to the amide recognition region composed of Ala318 and Asn152 in the binding pocket and are common functional patterns found in AmpC ligands.<sup>56,57</sup> The above analysis indicates that the SILCS-Pharm models are able to qualitatively reproduce important features known to be required for the binding of ligands to the eight targets. In addition, the FGFE ranking is an indicator of the importance of a feature for binding.

**Feature Prioritization Using FGFE.** Receptor-based pharmacophore modeling methods usually first generate all possible pharmacophore elements on the protein target surface and then, using various approaches (e.g., hydration site analysis<sup>7</sup>), select a subset for use in VS. In SILCS-Pharm, the FGFE may be used to prioritize identified features. Here, we quantitatively test the use of FGFE. Assuming three key pharmacophore feature models, all possible combinations out



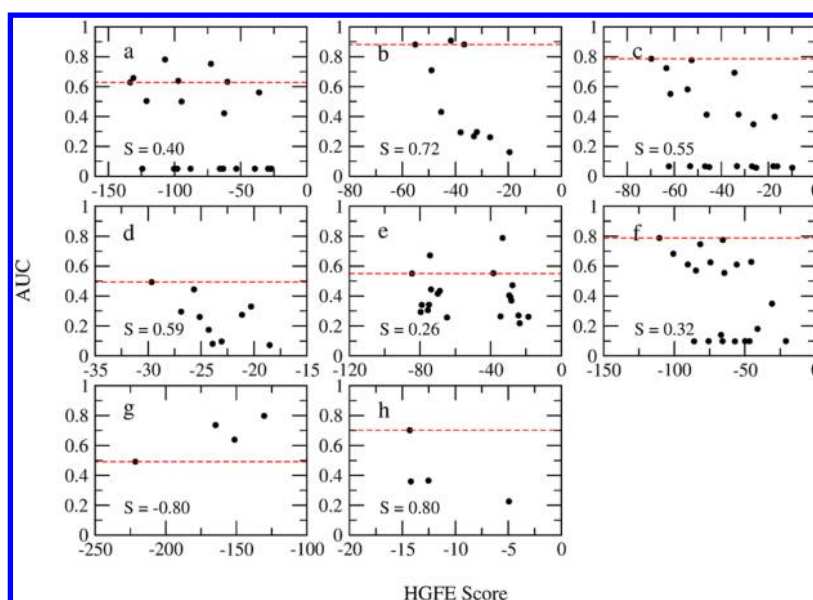


**Figure 4.** Relationship between HGFEs of all possible pharmacophore models containing three features and AUCs from VS for each target. (a) HIVPR; (b) FXa; (c) DHFR; (d) FGFR1; (e) P38 MAP; (f) ADA; (g) ER; (h) AmpC. The Spearman correlation coefficients  $S$  are shown. The red dashed line represents the AUC value for the model with the most favorable HGFE for each target.

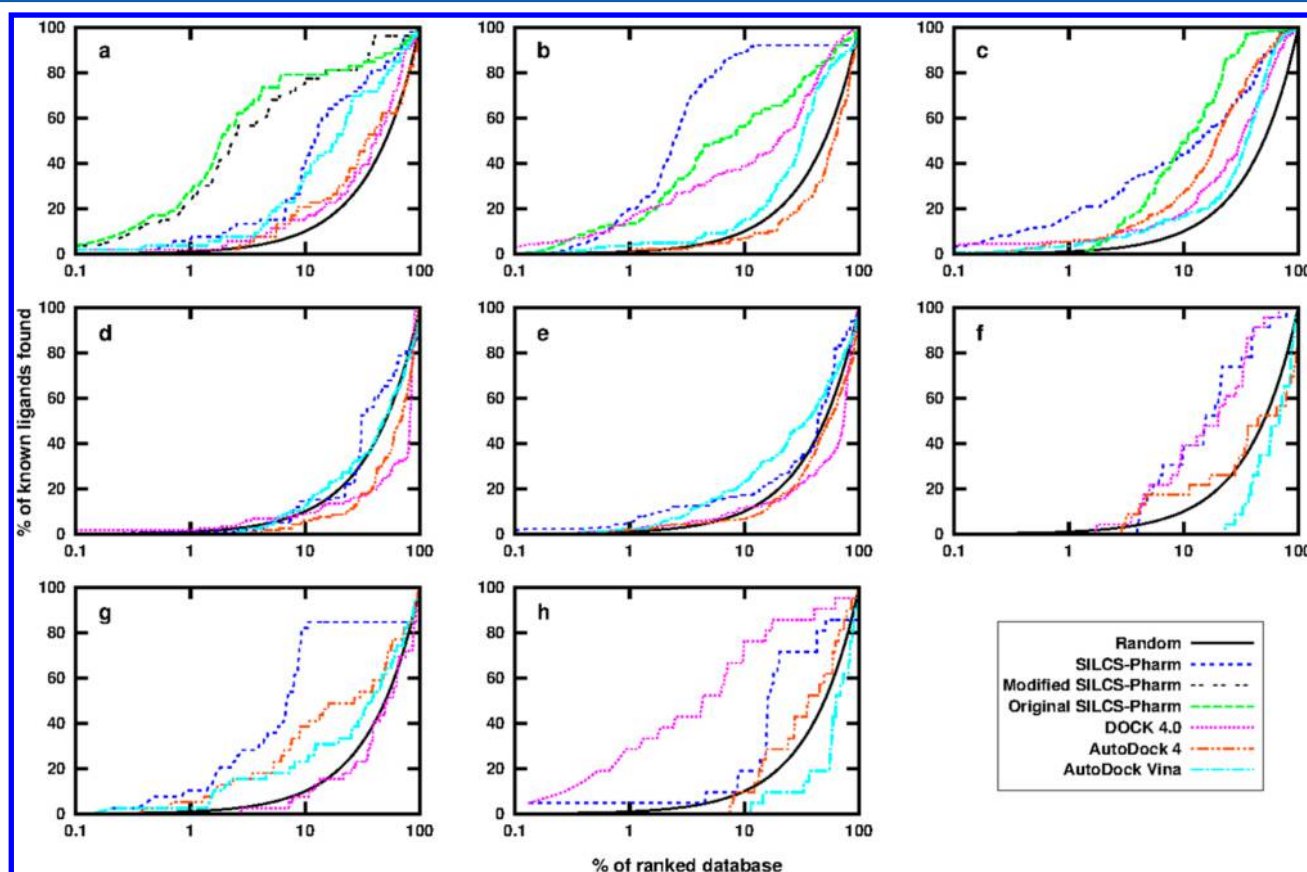


**Figure 5.** Enrichment plots of the SILCS pharmacophore modeling using DUD data sets for the eight protein targets: (a) HIVPR; (b) FXa; (c) DHFR; (d) FGFR1; (e) P38 MAP; (f) ADA; (g) ER; (h) AmpC. Results using DOCK 4.0, AutoDock 4 and AutoDock Vina are also shown for comparison. For the first three targets, the results from our former SILCS-Pharm study are shown. The black line indicates random selection of compounds from the database. The  $x$ -axis is in logarithmic scale to show the early stage performance more clearly.

of the total number of SILCS-Pharm identified features (Table S2 in the Supporting Information) were considered for each target and VS was performed using all constructed models under full matching mode. The AUC for each VS was then

evaluated and used to rank the model quality. Relationships between the hypothesis GFE (HGFE, which is the sum of FGFEs of all features in a model) and AUC were then plotted to investigate if the FGFE can serve as an indicator of feature



Table 4. Comparison of Enrichments for Different Docking and Pharmacophore Modeling Methods

targets	methods	EF <sub>1</sub>	EF <sub>10</sub>	EF <sub>20</sub>	AUC
HIVPR	4F SILCS-Pharm <sup>a</sup>	6.7	4.1	3.6	0.78
	SF modified SILCS-Pharm <sup>b</sup>	77.1	9.2	4.4	0.89
	original SILCS-Pharm <sup>c</sup>	99.6	9.8	4.3	0.88
	DOCK 4.0	2.0	1.5	1.2	0.58
	AutoDock 4	0	2.1	1.5	0.56
	AutoDock Vina	4.2	3.6	2.8	0.73
	FPP <sup>d</sup>	9.3	4.7	3.5	0.81
	HSRP <sup>d</sup>				<0.80 <sup>e</sup>
FXa	4F SILCS-Pharm <sup>a</sup>	41.9	11.4	5.1	0.91
	original SILCS-Pharm <sup>c</sup>	20.7	6.5	3.5	0.81
	DOCK 4.0	26.3	4.2	2.6	0.76
	AutoDock 4	0.7	0.7	0.7	0.42
	AutoDock Vina	3.8	1.5	1.6	0.64
	FPP <sup>d</sup>	12.2–29.7	5.6–6.7	3.5–3.9	0.81–0.87 <sup>f</sup>
	HSRP <sup>d</sup>				<0.83 <sup>e</sup>
DHFR	3F SILCS-Pharm <sup>a</sup>	29.3	4.8	3.0	0.79
	original SILCS-Pharm <sup>c</sup>	0.0	5.5	4.0	0.87
	DOCK 4.0	6.3	1.8	1.8	0.66
	AutoDock 4	6.3	2.8	2.8	0.76
	AutoDock Vina	3.8	1.7	1.2	0.65
	FPP <sup>d</sup>	2.0	1.5	1.3	0.51
	HSRP <sup>d</sup>				<0.62 <sup>e</sup>
FGFr1	3F SILCS-Pharm <sup>a</sup>	0.8	1.5	0.8	0.55
	DOCK 4.0	1.7	0.8	0.7	0.33
	AutoDock 4	0.0	0.6	0.4	0.38
	AutoDock Vina	0.0	1.2	1.2	0.50
P38 MAP	3F SILCS-Pharm <sup>a</sup>	6.4	1.8	1.3	0.57
	DOCK 4.0	2.0	1.1	0.7	0.39
	AutoDock 4	2.0	0.7	0.8	0.45
	AutoDock Vina	2.5	2.4	1.8	0.59
ADA	3F SILCS-Pharm <sup>a</sup>	0.0	3.8	3.0	0.80
	DOCK 4.0	0.0	4.3	2.7	0.79
	AutoDock 4	0.0	1.8	1.3	0.46
	AutoDock Vina	0.0	0.0	0.0	0.36
ERantagonist	4F SILCS-Pharm <sup>a</sup>	14.3	10.3	4.6	0.81
	DOCK 4.0	0.0	0.8	0.8	0.46
	AutoDock 4	6.0	4.2	2.5	0.64
	AutoDock Vina	2.8	2.4	1.7	0.59
AmpC	3F SILCS-Pharm <sup>a</sup>	5.0	2.0	3.6	0.70
	DOCK 4.0	104.6	9.5	4.7	0.87
	AutoDock 4	0.0	1.0	1.4	0.58
	AutoDock Vina	0.0	0.0	0.5	0.35

<sup>a</sup>The results of the best performing SILCS pharmacophore model based on AUC with a specific number of key features (e.g., 4F means 4 top FGFE ranked features are considered as key features in the model) are shown. <sup>b</sup>The best modified model for HIVPR with the POS feature changed into a HBDON|POS feature. <sup>c</sup>The best results from the original SILCS-Pharm work.<sup>16</sup> <sup>d</sup>Full Protein Pharmacophore (FPP) and Hydration Site Restricted Pharmacophore (HSRP) results from Lill and co-workers work.<sup>7</sup> <sup>e</sup>The upper AUC values for HSRP models using different parameters are estimated from Figure 7 in ref 7, as no exact values were reported. <sup>f</sup>Three protein structures were used for FXa in ref 7, so the range of AUC values is shown here.

importance and thereby be used to select a pharmacophore model for VS. Figure 4 presents the AUC values as a function of the HGFE scores for three key feature containing pharmacophore models. Analysis of models with larger numbers of features was not done as ER and AmpC only have four available features. In general, the most favorable pharmacophore model based on the HGFE scores is among the top models as ranked by AUC. The most significant exceptions occur with HIVPR, P38 MAP and ER. The results with HIVPR (Figure 4a) may have contributions from the protonation state of the Asp residues in the catalytic site (see above) whereas the known conformational flexibility of P38 MAP may play a role in

that protein (Figure 4e). However, in both cases, the top scoring model based on HGFE is among the top three or four AUC-ranked models. The discrepancy with ER may be associated with the small number of models (Figure 4g). We note that the correlations are generally quite poor, as reflected by the low correlation coefficient values, which may be indicative of individual pharmacophore features being poor predictors of active compounds. For example, in the case of HIVPR, many of the models with favorable HGFEs have AUC values that are under 0.1. All of these models contain the POS feature which was discussed above as an inappropriate feature for the target. Thus, although the correlations are generally

**Table 5. Percentage Loss (%) of AUC Using the Best Performing Model as Listed in Table 4 without Complementary Features or without Volume Constraints for Each Target**

targets	HIVPR	FXa	DHFR	FGFr1	P38 MAP	ADA	ERantagonist	AmpC
without complementary features	0	0	0	0	2	0	— <sup>a</sup>	0
without volume constraints	1	0	0	11	2	1	0	0

<sup>a</sup>The best model for ER contains all four identified features and thus all features are key features, such that models without complementary features cannot be created.

weak, the overall ability of HGFE scores to yield high AUC values is satisfactory, indicating its utility in selecting pharmacophore models for VS. Accordingly, this approach was used for the final analysis.

**VS Using SILCS Pharmacophore Models.** SILCS pharmacophore models were tested in VS using DUD data sets for the eight proteins listed in Table 2. The models for each target contain all identified SILCS pharmacophore features and volume constraints with the number of key features varying. The tested models were chosen to have at least three key features and only those features with the most favorable FGFE are labeled as key features. For example, if four features are identified for a target, then a 3-key features model is a model where the three top FGFE ranked features are assigned as key features. And it is possible to have all the features in a model assigned as key features. Accordingly, a total of  $N-2$  models for a target that has  $N$  identified features can be constructed and tested in VS under partial matching mode.

As the pharmacophore generation scheme presented in the preceding paragraph allows for the creation of multiple models, enrichment performance for all possible models was determined for each target. As shown in Table S3 of the Supporting Information, that range of variability is significant. In all cases, the choice of 3 or 4 key features yields the highest enrichment whereas the use of 5 or more key features leads to a significant decrease in enrichment. Thus, in situations where no priori information on active ligands is available, there is the possibility of selecting a less than ideal model for VS, though the selection of 3 or 4 key features is recommended. In addition, as presented below, the use of LGFE reranking leads to the selection of alternate active ligands versus the use of RMSD selection alone, suggesting that both approaches should be used and the results combined when selecting compounds for experimental assays. The remainder of the manuscript focuses on the best performing model for each target.

Enrichment results for the best performing pharmacophore model are shown in Figure 5 and Table 4 and compared with docking results using available docking programs. For the first three targets, the results using the extended SILCS-Pharm protocol were also compared with previously reported VS results using the original SILCS-Pharm protocol.<sup>16</sup> In addition, comparisons are made with available results from Lill and co-workers' work.<sup>7</sup>

For HIVPR, the best pharmacophore model has four key features and its performance is slightly worse than the best previous results using the original SILCS-Pharm protocol. However, the best previous model contained 6 features, whereas the original 4-feature model, which has the four hydrophobic features, had significantly worse performance ( $EF_1 = 2.0$ ,  $EF_{10} = 2.1$ ,  $EF_{20} = 1.4$ ,  $AUC = 0.56$ ) than the new 4-feature model. This is due to the features from the new SILCS-Pharm being more accurately defined than in the original method. As discussed above, the fifth feature, POS, in the current model may not be suitable due to both the catalytic Asp

residues being charged in the SILCS simulations, whereas one of the residues is likely neutral which would favor a neutral HBDON feature in that region.<sup>44</sup> Accordingly, we tested a modified model with feature POS being changed to HBDON/POS to allow the matching of both neutral and charged donors at this location. The resulting 5-feature model has a similar performance as the best original model, emphasizing the importance of the protonation state selected for the SILCS simulation. For FXa, the new model has better performance than the original SILCS-Pharm model, as indicated by the increased EFs and AUC. For DHFR, concerns about the zero value for  $EF_1$  existed in the original SILCS-Pharm study, but this is no longer an issue in the new model where  $EF_1 = 29.3$ , though the AUC is slightly worse than the original result. These results indicate that the extended SILCS-Pharm model shows more robust performance versus the original SILCS-Pharm results, indicating the advantage of using multiple probe molecules during pharmacophore model development.

The quality of the extended SILCS-Pharm approach was further validated by comparing results with those from DOCK 4.0, AutoDock 4 and AutoDock Vina. For all the targets tested, except AmpC, SILCS-Pharm outperformed the three docking programs, as reflected by the larger EF and AUC values. For AmpC, though SILCS-Pharm yielded better results than the two AutoDock programs, it was outperformed by DOCK 4.0. It is interesting to note that the DOCK 3.5 result for AmpC presented in the DUD paper was worse than the current SILCS-Pharm result. The improved result for AmpC using DOCK 4.0 may be due to the use of the in-house developed docking protocol,<sup>38,39</sup> where the CHARMM parameters<sup>30</sup> instead of the original DOCK parameters are used to determine the binding energy and guide the docking.

**Complementary Features and Volume Constraints.** Although the success of the extended SILCS-Pharm may be largely attributed to the use of multiple solute types in the SILCS simulation, the use of complementary features and volume constraints may also contribute to the improved VS results. The contributions by these two factors were tested by using models in their absence for VS. For each target, the best performing model was considered and two new models were created with removal of either the complementary features or the volume constraints and tested in VS. Table 5 lists the percentage loss on the AUC value using the two modified models compared with the full model for each target. Though generally not large, some decreases in the AUCs occurred for some targets when the complementary features or the volume constraints were absent suggesting that the two factors indeed helped with enrichment during VS. The observed small change may be due to the DUD data sets being designed to have decoys that have physiochemical properties similar to the ligands, such that the sizes and functional features of the ligands and decoys for each target are similar. Thus, the complementary features used to select ligands with more matches and the volume constraints used to avoid oversized compounds that



Table 6. AUCs Using RMSD, SP LGFE and SILCS-MC Sampled LGFE for Ranking for the Eight Targets<sup>a</sup>

ranking score	HIVPR		FXa		DHFR		FGFr1		P38 MAP		ADA		ER		AmpC	
	AUC	D% <sup>a</sup>	AUC	D% <sup>a</sup>	AUC	D% <sup>a</sup>	AUC	D% <sup>a</sup>	AUC	D% <sup>a</sup>	AUC	D% <sup>a</sup>	AUC	D% <sup>a</sup>	AUC	D% <sup>a</sup>
RMSD	0.78		0.91		0.79		0.55		0.57		0.80		0.81		0.70	
SP LGFE	0.54	4	0.78	8	0.67	9	0.75	14	0.75	43	0.58	4	0.86	46	0.55	0
MC LGFE	0.49	2	0.90	17	0.70	6	0.66	13	0.73	30	0.64	0	0.83	41	0.62	0

<sup>a</sup>D% is the percentage of different active ligands in the top 10% ranked compounds identified by LGFE score that were not identified by RMSD score.  $D\% = N_{\text{diff}}/N_{\text{ligands}} \times 100\%$ , where  $N_{\text{diff}}$  is the number of active ligands identified by LGFE score among the top 10% LGFE ranked compounds that are not found by RMSD score among the top 10% RMSD ranked compounds, and  $N_{\text{ligands}}$  are the total number of active ligands in the database for the target.

Table 7. Percentage of Active Ligands Identified<sup>a</sup> in the Top 10% Ranked Compounds Using RMSD, Single Point LGFE and SILCS-MC Sampled LGFE Ranking Alone as well as the Consensus Ranking Using both RMSD and LGFE for the Eight Targets

ranking score	HIVPR	FXa	DHFR	FGFr1	P38 MAP	ADA	ER	AmpC
RMSD	38	25	44	14	17	39	38	10
SP LGFE	19	11	20	16	48	4	85	0
MC LGFE	11	22	20	13	33	4	77	0
RMSD + SP LGFE	42	33	53	29	60	43	85	10
RMSD + MC LGFE	40	42	50	27	47	39	79	10

<sup>a</sup>Percentage of active ligands =  $N_{\text{ligands in 10\%}}/N_{\text{ligands}} \times 100\%$ , where  $N_{\text{ligands in 10\%}}$  is the number of active ligands identified among the top 10% ranked compounds and  $N_{\text{ligands}}$  is the total number of active ligands in the database for the target.

do not fit into the binding site have limited roles in compound selection in this case. However, it is anticipated that the two terms will make additional contributions in practical use, where compounds with very dissimilar properties and shapes are being screened. Moreover, given that the new terms do not add much additional computational cost to VS, even a relatively small improvement warrants their inclusion. For example, VS against the 5745 decoys of FXa took 190 and 170 s, respectively, using pharmacophore models with and without volume constraints.

**LGFE Reranking.** Though for most test cases, an AUC of more than 0.7 was observed when using SILCS-Pharm, low AUCs were found for two targets. These two targets, FGFr1 and P38 MAP, show an AUC lower than 0.6 implying the two targets are challenging cases for VS, which is also consistent with the previous DUD docking results ( $EF_1$  is 0 and 2.1).<sup>22</sup> As shown in Figure 3 and discussed above, the SILCS-Pharm features for these two targets are consistent with the binding modes of the known ligands. This suggests the features in the pharmacophore model are appropriate for VS and should be able to identify the known ligands and differentiate them from decoys. The poor performance may thus imply that the RMSD score used to rank compounds is inadequate. Previously, LGFE, which is the sum of all atom GFE scores for a ligand, was proposed for scoring and shown to reproduce various experimental binding affinity data sets satisfactorily.<sup>18,20,25</sup> Here, normalized LGFE was used to rerank the obtained pharmacophore RMSD-selected conformations from SILCS-Pharm VS for all the targets and to determine if the use of LGFE ranking leads to improvements in the enrichment. Calculation of the LGFE scores is defined in eq 2. The current scoring represents a refinement of that previously reported<sup>25</sup> with no weighting factors being used, the scores being normalized for the number of classified versus total non-hydrogen atoms in the compound and new definitions of the atom types based only on nonhydrogen atoms as presented in Table S4 of the Supporting Information are used. In addition to SP LGFE scores based on the RMSD-selected conformation, local relaxation of the ligands was performed using GFE-based

SILCS-MC sampling<sup>25</sup> from which Boltzmann-averaged LGFE scores were obtained.

Table 6 shows the AUCs for the results with ligand ranking based on SP LGFE scores, SILCS-MC sampled LGFE score and the RMSD criteria. For the two worst RMSD-based ranking cases, FGFr1 and P38 MAP, the SP LGFE reranking improves the enrichment with AUCs increased from 0.55 to 0.75 for FGFr1 and from 0.57 to 0.75 for P38 MAP. For most of the other cases, similar or slightly worse results are seen when using SP LGFE reranking. Similarly, use of the relaxed SILCS-MC LGFE scores yielded ambiguous results with respect to the RMSD and SP LGFE scores. For HIVPR, the heavily decreased performance using LGFE for scoring is likely again due to the wrong protonation state used for the SILCS simulations as described before.

Given ambiguous results associated with LGFE ranking, analysis was undertaken to test if LGFE ranking may identify alternate ligands with a high probability of binding to the target protein versus those from RMSD ranking alone. Included in Table 6 is the percentage of different ligands identified using LGFE ranking versus RMSD ranking ( $D\%$ ). In the majority of cases, alternate ligands are being identified by the use of LGFE scores. This result suggests that the most optimal approach for the selection of ligands in a practical VS would be a combination of ligands from RMSD and LGFE rankings. To test this, the top 10% of the ranked compounds from RMSD or LGFE scoring were obtained and the percentage of active ligands among those compounds determined (i.e., if all the active compounds were found in the top 10%, the result would be 100 in Table 7). RMSD and LGFE results were combined by simply taking the top 10% list from both rankings and determining the number of active compounds among the combined set. As shown in Table 7, the combination of RMSD- and LGFE-based ranking always yielded an equivalent or larger percentage of active ligands over the individual methods. This result is consistent with previous findings about consensus scoring<sup>58</sup> that the identification of true positives is enhanced and more diverse sets of ligands are identified using consensus ranking. Concerning computational costs, taking P38 MAP for

example, which includes 454 ligands, the SP LGFE calculations required 2700 CPU seconds using a single core on an AMD Opteron 2350 processor equipped node while the 5000 steps SILCS-MC sampled LGFEs required almost the same amount of calculation time. Thus, it is recommended that the final selection of compounds be based on the combined final top ranked lists from RMSD and LGFE ranking, with the SP LGFE scores yielding the greatest improvement with the exception of FXa.

## CONCLUSION

Using additional solutes in the SILCS simulations enables the SILCS-Pharm protocol to be extended and reformulated. Advantages over the original approach were validated using eight protein targets with their DUD test sets. The new protocol not only defines the pharmacophore features more accurately by including explicit hydrogen bond donor and acceptor solutes but also includes more specific features, allowing for the definition of more feature types. With the use of complementary features and volume constraints, the VS results show that the extended SILCS-Pharm improves upon the original protocol and outperforms three commonly used docking programs in most cases suggesting its potential utility for CADD. Single point- and SILCS-MC sampling-based LGFE rerankings, which introduce energetic criteria into compound ranking, were tested and shown to enhance the SILCS-Pharm results with respect to the identification of alternate ligands for experimental assay. Thus, as pharmacophore-based VS is very efficient and far less time-consuming than other VS methods, SILCS-Pharm can be considered for use in CADD projects when screening a large databases of compounds as well as to facilitate ligand docking in general. Furthermore, given the capability of the SILCS approach to facilitate ligand optimization,<sup>18,20,25</sup> which would be performed using the same GFE FragMaps as used for the SILCS-Pharm, the overall economy and utility of the SILCS approach in ligand design may be significant.

## ASSOCIATED CONTENT

### Supporting Information

Overlap coefficients used to check convergences of the SILCS simulations, GFE cutoffs used to develop SILCS pharmacophore features, enrichment performances for all pharmacophore models of the eight tested targets, set of rules for conversion between CGenFF atom types and SILCS FragMap types for LGFE calculation, and figure showing SILCS exclusion maps for all eight tested targets. This material is available free of charge via the Internet at <http://pubs.acs.org>.

## AUTHOR INFORMATION

### Corresponding Author

\*A. D. MacKerell, Jr. E-mail: [alex@outerbanks.umaryland.edu](mailto:alex@outerbanks.umaryland.edu).

### Notes

The authors declare the following competing financial interest(s): A.D.M., Jr. is co-founder and chief scientific officer of SilcsBio LLC.

## ACKNOWLEDGMENTS

This work was supported by NIH grant CA107331, Maryland Industrial Partnerships Award 5212, University of Maryland Center for Biomolecular Therapeutics and the Samuel Waxman Cancer Research Foundation. The authors acknowledge

computer time and resources from the Computer-Aided Drug Design (CADD) Center at the University of Maryland, Baltimore.

## REFERENCES

- (1) Yu, W.; Guvench, O.; MacKerell, A. D. Computational Approaches for the Design of Protein–Protein Interaction Inhibitors. In *Understanding and Exploiting Protein–Protein Interactions as Drug Targets*; Zinzalla, G., Ed.; Future Science Ltd.: London, U. K., 2013; pp 99–102.
- (2) Zhong, S.; Oashi, T.; Yu, W.; Shapiro, P.; MacKerell, A. D. Prospects of Modulating Protein–Protein Interactions. In *Protein–Ligand Interactions*; Gohlke, H., Ed.; Wiley KGaA: Weinheim, Germany, 2012; pp 295–329.
- (3) Leach, A. R.; Gillet, V. J.; Lewis, R. A.; Taylor, R. Three-Dimensional Pharmacophore Methods in Drug Discovery. *J. Med. Chem.* **2009**, *53*, 539–558.
- (4) Yang, S. Y. Pharmacophore Modeling and Applications in Drug Discovery: Challenges and Recent Advances. *Drug Discovery Today* **2010**, *15*, 444–450.
- (5) Joseph-McCarthy, D.; Alvarez, J. C. Automated Generation of MCSS-Derived Pharmacophoric DOCK Site Points for Searching Multiconformation Databases. *Proteins: Struct., Funct., Bioinf.* **2003**, *51*, 189–202.
- (6) Cross, S.; Baroni, M.; Goracci, L.; Cruciani, G. GRID-based Three-Dimensional Pharmacophores I: FLAPPharm, A Novel Approach for Pharmacophore Elucidation. *J. Chem. Inf. Model.* **2012**, *52*, 2587–2598.
- (7) Hu, B.; Lill, M. A. Protein Pharmacophore Selection Using Hydration-Site Analysis. *J. Chem. Inf. Model.* **2012**, *52*, 1046–1060.
- (8) Kurczab, R.; Bojarski, A. J. New Strategy for Receptor-based Pharmacophore Query Construction: A Case Study for 5-HT<sub>7</sub> Receptor Ligands. *J. Chem. Inf. Model.* **2013**, *53*, 3233–3243.
- (9) Indarte, M. n.; Liu, Y.; Madura, J. D.; Surratt, C. K. Receptor-based Discovery of a Plasmalemmal Monoamine Transporter Inhibitor via High-Throughput Docking and Pharmacophore Modeling. *ACS Chem. Neurosci.* **2010**, *1*, 223–233.
- (10) Deng, J.; Lee, K. W.; Sanchez, T.; Cui, M.; Neamati, N.; Briggs, J. M. Dynamic Receptor-Based Pharmacophore Model Development and Its Application in Designing Novel HIV-1 Integrase Inhibitors. *J. Med. Chem.* **2005**, *48*, 1496–1505.
- (11) Lerner, M. G.; Bowman, A. L.; Carlson, H. A. Incorporating Dynamics in *E. coli* Dihydrofolate Reductase Enhances Structure-based Drug Discovery. *J. Chem. Inf. Model.* **2007**, *47*, 2358–2365.
- (12) Guha, S.; Majumbar, D. Effect of Hydration on the Conformational Properties and Pharmacophoric Pattern of Several GABA Mediators. *J. Mol. Struct.: THEOCHEM* **1992**, *257*, 451–473.
- (13) Bowman, A. L.; Makriyannis, A. Approximating Protein Flexibility through Dynamic Pharmacophore Models: Application to Fatty Acid Amide Hydrolase (FAAH). *J. Chem. Inf. Model.* **2011**, *51*, 3247–3253.
- (14) Xu, L.; Zhou, S.; Yu, K.; Gao, B.; Jiang, H.; Zhen, X.; Fu, W. Molecular Modeling of the 3D Structure of 5-HT<sub>1A</sub>R: Discovery of Novel 5-HT<sub>1A</sub>R Agonists via Dynamic Pharmacophore-based Virtual Screening. *J. Chem. Inf. Model.* **2013**, *53*, 3202–3211.
- (15) Thangapandian, S.; John, S.; Lee, Y.; Kim, S.; Lee, K. W. Dynamic Structure-based Pharmacophore Model Development: A New and Effective Addition in the Histone Deacetylase 8 (HDAC8) Inhibitor Discovery. *Int. J. Mol. Sci.* **2011**, *12*, 9440–9462.
- (16) Yu, W.; Lakkaraju, S.; Raman, E. P.; MacKerell, A., Jr. Site-Identification by Ligand Competitive Saturation (SILCS) Assisted Pharmacophore Modeling. *J. Comput.-Aided. Mol. Des.* **2014**, *28*, 491–507.
- (17) Guvench, O.; MacKerell, A. D., Jr. Computational Fragment-based Binding Site Identification by Ligand Competitive Saturation. *PLoS Comput. Biol.* **2009**, *5*, e1000435.
- (18) Raman, E. P.; Yu, W.; Guvench, O.; MacKerell, A. D. Reproducing Crystal Binding Modes of Ligand Functional Groups



Using Site-Identification by Ligand Competitive Saturation (SILCS) Simulations. *J. Chem. Inf. Model.* **2011**, *51*, 877–896.

- (19) Raman, E. P.; Vanommeslaeghe, K.; MacKerell, A. D. Site-Specific Fragment Identification Guided by Single-Step Free Energy Perturbation Calculations. *J. Chem. Theory Comput.* **2012**, *8*, 3513–3525.
- (20) Cao, X.; Yap, J.; Newell-Rogers, M.; Peddaboina, C.; Jiang, W.; Papaconstantinou, H.; Jupiter, D.; Rai, A.; Jung, K.-Y.; Tubin, R.; Yu, W.; Vanommeslaeghe, K.; Wilder, P.; MacKerell, A.; Fletcher, S.; Smythe, R. The Novel BH3 Alpha-Helix Mimetic JY-1-106 Induces Apoptosis in a Subset of Cancer Cells (Lung Cancer, Colon Cancer and Mesothelioma) by Disrupting Bcl-xL and Mcl-1 Protein-Protein Interactions with Bak. *Mol. Cancer* **2013**, *12*, 42.
- (21) Foster, T. J.; MacKerell, A. D.; Guvench, O. Balancing Target Flexibility and Target Denaturation in Computational Fragment-based Inhibitor Discovery. *J. Comput. Chem.* **2012**, *33*, 1880–1891.
- (22) Huang, N.; Shoichet, B. K.; Irwin, J. J. Benchmarking Sets for Molecular Docking. *J. Med. Chem.* **2006**, *49*, 6789–6801.
- (23) Ewing, T. A.; Makino, S.; Skillman, A. G.; Kuntz, I. DOCK 4.0: Search Strategies for Automated Molecular Docking of Flexible Molecule Databases. *J. Comput.-Aided Mol. Des.* **2001**, *15*, 411–428.
- (24) Morris, G. M.; Huey, R.; Lindstrom, W.; Sanner, M. F.; Belew, R. K.; Goodsell, D. S.; Olson, A. J. AutoDock4 and AutoDockTools4: Automated Docking with Selective Receptor Flexibility. *J. Comput. Chem.* **2009**, *30*, 2785–2791.
- (25) Raman, E. P.; Yu, W.; Lakkaraju, S. K.; MacKerell, A. D. Inclusion of Multiple Fragment Types in the Site Identification by Ligand Competitive Saturation (SILCS) Approach. *J. Chem. Inf. Model.* **2013**, *53*, 3384–3398.
- (26) Trott, O.; Olson, A. J. AutoDock Vina: Improving the Speed and Accuracy of Docking With a New Scoring Function, Efficient Optimization, and Multithreading. *J. Comput. Chem.* **2010**, *31*, 455–461.
- (27) Bernstein, F. C.; Koetzle, T. F.; Williams, G. J. B.; Meyer, E. F., Jr.; Brice, M. D.; Rodgers, J. R.; Kennard, O.; Shimanouchi, T.; Tasumi, M. The Protein Data Bank: A Computer-based Archival File for Macromolecular Structures. *J. Mol. Biol.* **1977**, *112*, 535–542.
- (28) Word, J. M.; Lovell, S. C.; Richardson, J. S.; Richardson, D. C. Asparagine and Glutamine: Using Hydrogen Atom Contacts in the Choice of Side-Chain Amide Orientation. *J. Mol. Biol.* **1999**, *285*, 1735–1747.
- (29) Van Der Spoel, D.; Lindahl, E.; Hess, B.; Groenhof, G.; Mark, A. E.; Berendsen, H. J. C. GROMACS: Fast, Flexible, and Free. *J. Comput. Chem.* **2005**, *26*, 1701–1718.
- (30) MacKerell, A. D.; Bashford, D.; Bellott, M.; Dunbrack, R. L.; Evanseck, J. D.; Field, M. J.; Fischer, S.; Gao, J.; Guo, H.; Ha, S.; Joseph-McCarthy, D.; Kuchnir, L.; Kucsera, K.; Lau, F. T. K.; Mattos, C.; Michnick, S.; Ngo, T.; Nguyen, D. T.; Prodhom, B.; Reiher, W. E.; Roux, B.; Schlenkrich, M.; Smith, J. C.; Stote, R.; Straub, J.; Watanabe, M.; Wiórkiewicz-Kucsera, J.; Yin, D.; Karplus, M. All-Atom Empirical Potential for Molecular Modeling and Dynamics Studies of Proteins. *J. Phys. Chem. B* **1998**, *102*, 3586–3616.
- (31) Mackerell, A. D.; Feig, M.; Brooks, C. L. Extending the Treatment of Backbone Energetics in Protein Force Fields: Limitations of Gas-Phase Quantum Mechanics in Reproducing Protein Conformational Distributions in Molecular Dynamics Simulations. *J. Comput. Chem.* **2004**, *25*, 1400–1415.
- (32) Vanommeslaeghe, K.; Hatcher, E.; Acharya, C.; Kundu, S.; Zhong, S.; Shim, J.; Darian, E.; Guvench, O.; Lopes, P.; Vorobyov, I.; Mackerell, A. D. CHARMM General Force Field: A Force Field for Drug-Like Molecules Compatible with the CHARMM All-Atom Additive Biological Force Fields. *J. Comput. Chem.* **2010**, *31*, 671–690.
- (33) Yu, W.; He, X.; Vanommeslaeghe, K.; MacKerell, A. D. Extension of the CHARMM General Force Field to Sulfonfyl-Containing Compounds and Its Utility in Biomolecular Simulations. *J. Comput. Chem.* **2012**, *33*, 2451–2468.
- (34) Jorgensen, W. L.; Chandrasekhar, J.; Madura, J. D.; Impey, R. W.; Klein, M. L. Comparison of Simple Potential Functions for Simulating Liquid Water. *J. Chem. Phys.* **1983**, *79*, 926–935.
- (35) Durell, S. R.; Brooks, B. R.; Ben-Naim, A. Solvent-Induced Forces between Two Hydrophilic Groups. *J. Phys. Chem.* **1994**, *98*, 2198–2202.
- (36) *Molecular operating environment (MOE)*, version 2012.10; Chemical Computing Group Inc.: Montreal, Canada, 2012.
- (37) Halgren, T. A. Merck Molecular Force Field. I. Basis, Form, Scope, Parameterization, and Performance of MMFF94. *J. Comput. Chem.* **1996**, *17*, 490–519.
- (38) Zhong, S.; Chen, X.; Zhu, X.; Dziegielewska, B.; Bachman, K. E.; Ellenberger, T.; Ballin, J. D.; Wilson, G. M.; Tomkinson, A. E.; MacKerell, A. D. Identification and Validation of Human DNA Ligase Inhibitors Using Computer-Aided Drug Design. *J. Med. Chem.* **2008**, *51*, 4553–4562.
- (39) Cerchiatti, L. C.; Ghetu, A. F.; Zhu, X.; Da Silva, G. F.; Zhong, S.; Matthews, M.; Bunting, K. L.; Polo, J. M.; Farès, C.; Arrowsmith, C. H.; Yang, S. N.; Garcia, M.; Coop, A.; MacKerell, A. D., Jr.; Privé, G. G.; Melnick, A. A Small-Molecule Inhibitor of BCL6 Kills DLBCL Cells in Vitro and in Vivo. *Cancer Cell* **2010**, *17*, 400–411.
- (40) Morris, G. M.; Goodsell, D. S.; Halliday, R. S.; Huey, R.; Hart, W. E.; Belew, R. K.; Olson, A. J. Automated Docking Using a Lamarckian Genetic Algorithm and an Empirical Binding Free Energy Function. *J. Comput. Chem.* **1998**, *19*, 1639–1662.
- (41) Zweig, M. H.; Campbell, G. Receiver-Operating Characteristic (ROC) Plots: A Fundamental Evaluation Tool in Clinical Medicine. *Clin. Chem.* **1993**, *39*, 561–577.
- (42) Lam, P. Y.; Jadhav, P. K.; Eyermann, C. J.; Hodge, C. N.; Ru, Y.; Bacheler, L. T.; Meek, J. L.; Otto, M. J.; Rayner, M. M.; Wong, Y. N.; et al. Rational Design of Potent, Bioavailable, Nonpeptide Cyclic Ureas as HIV Protease Inhibitors. *Science* **1994**, *263*, 380–384.
- (43) Schaal, W.; Karlsson, A.; Ahlsén, G.; Lindberg, J.; Andersson, H. O.; Danielson, U. H.; Classon, B.; Unge, T.; Samuelsson, B.; Hultén, J.; Hallberg, A.; Karlén, A. Synthesis and Comparative Molecular Field Analysis (CoMFA) of Symmetric and Nonsymmetric Cyclic Sulfamide HIV-1 Protease Inhibitors. *J. Med. Chem.* **2000**, *44*, 155–169.
- (44) Smith, R.; Brereton, I. M.; Chai, R. Y.; Kent, S. B. H. Ionization States of the Catalytic Residues in HIV-1 Protease. *Nat. Struct. Mol. Biol.* **1996**, *3*, 946–950.
- (45) Adler, M.; Davey, D. D.; Phillips, G. B.; Kim, S.-H.; Jancarik, J.; Rumennik, G.; Light, D. R.; Whitlow, M. Preparation, Characterization, and the Crystal Structure of the Inhibitor ZK-807834 (CI-1031) Complexed with Factor Xa. *Biochemistry* **2000**, *39*, 12534–12542.
- (46) Maignan, S.; Guilloteau, J.-P.; Pouzieux, S.; Choi-Sledeski, Y. M.; Becker, M. R.; Klein, S. I.; Ewing, W. R.; Pauls, H. W.; Spada, A. P.; Mikol, V. Crystal Structures of Human Factor Xa Complexed with Potent Inhibitors. *J. Med. Chem.* **2000**, *43*, 3226–3232.
- (47) Bolin, J. T.; Filman, D. J.; Matthews, D. A.; Hamlin, R. C.; Kraut, J. Crystal Structures of *Escherichia coli* and *Lactobacillus casei* Dihydrofolate Reductase Refined at 1.7 Å Resolution. I. General Features and Binding of Methotrexate. *J. Biol. Chem.* **1982**, *257*, 13650–13662.
- (48) Guagnano, V.; Furet, P.; Spanka, C.; Bordas, V.; Le Douget, M.; Stamm, C.; Brueggen, J.; Jensen, M. R.; Schnell, C.; Schmid, H.; Wartmann, M.; Berghausen, J.; Drueckes, P.; Zimmerlin, A.; Bussiere, D.; Murray, J.; Graus Porta, D. Discovery of 3-(2,6-Dichloro-3,5-dimethoxy-phenyl)-1-{6-[4-(4-ethyl-piperazin-1-yl)-phenylamino]-pyrimidin-4-yl}-1-methyl-urea (NVP-BGJ398), A Potent and Selective Inhibitor of the Fibroblast Growth Factor Receptor Family of Receptor Tyrosine Kinase. *J. Med. Chem.* **2011**, *54*, 7066–7083.
- (49) Fitzgerald, C. E.; Patel, S. B.; Becker, J. W.; Cameron, P. M.; Zaller, D.; Pikounis, V. B.; O’Keefe, S. J.; Scapin, G. Structural basis for p38[α] MAP Kinase Quinazolinone and Pyridol-Pyrimidine Inhibitor Specificity. *Nat. Struct. Mol. Biol.* **2003**, *10*, 764–769.
- (50) Wang, Z.; Canagarajah, B. J.; Boehm, J. C.; Kassisa, S.; Cobb, M. H.; Young, P. R.; Abdel-Meguid, S.; Adams, J. L.; Goldsmith, E. J. Structural Basis of Inhibitor Selectivity in MAP Kinases. *Structure* **1998**, *6*, 1117–1128.
- (51) Shewchuk, L.; Hassell, A.; Wisely, B.; Rocque, W.; Holmes, W.; Veal, J.; Kuyper, L. F. Binding Mode of the 4-Anilinoquinazoline Class

of Protein Kinase Inhibitor: X-ray Crystallographic Studies of 4-Anilinoquinazolines Bound to Cyclin-Dependent Kinase 2 and p38 Kinase. *J. Med. Chem.* **1999**, *43*, 133–138.

(52) Terasaka, T.; Kinoshita, T.; Kuno, M.; Nakanishi, I. A Highly Potent Non-Nucleoside Adenosine Deaminase Inhibitor: Efficient Drug Discovery by Intentional Lead Hybridization. *J. Am. Chem. Soc.* **2003**, *126*, 34–35.

(53) Terasaka, T.; Kinoshita, T.; Kuno, M.; Seki, N.; Tanaka, K.; Nakanishi, I. Structure-Based Design, Synthesis, and Structure–Activity Relationship Studies of Novel Non-nucleoside Adenosine Deaminase Inhibitors. *J. Med. Chem.* **2004**, *47*, 3730–3743.

(54) Shiau, A. K.; Barstad, D.; Loria, P. M.; Cheng, L.; Kushner, P. J.; Agard, D. A.; Greene, G. L. The Structural Basis of Estrogen Receptor/Coactivator Recognition and the Antagonism of This Interaction by Tamoxifen. *Cell* **1998**, *95*, 927–937.

(55) Blizzard, T. A.; DiNinno, F.; Morgan, J. D., II; Chen, H. Y.; Wu, J. Y.; Kim, S.; Chan, W.; Birzin, E. T.; Yang, Y. T.; Pai, L.-Y.; Fitzgerald, P. M. D.; Sharma, N.; Li, Y.; Zhang, Z.; Hayes, E. C.; DaSilva, C. A.; Tang, W.; Rohrer, S. P.; Schaeffer, J. M.; Hammond, M. L. Estrogen Receptor Ligands. Part 9: Dihydrobenzoxathiin SERAMs with Alkyl Substituted Pyrrolidine Side Chains and Linkers. *Bioorg. Med. Chem. Lett.* **2005**, *15*, 107–113.

(56) Powers, R. A.; Morandi, F.; Shoichet, B. K. Structure-based Discovery of a Novel, Noncovalent Inhibitor of AmpC  $\beta$ -Lactamase. *Structure* **2002**, *10*, 1013–1023.

(57) Tondi, D.; Morandi, F.; Bonnet, R.; Costi, M. P.; Shoichet, B. K. Structure-based Optimization of a Non- $\beta$ -lactam Lead Results in Inhibitors That Do Not up-Regulate  $\beta$ -Lactamase Expression in Cell Culture. *J. Am. Chem. Soc.* **2005**, *127*, 4632–4639.

(58) Wang, R.; Wang, S. How Does Consensus Scoring Work for Virtual Library Screening? An Idealized Computer Experiment. *J. Chem. Inf. Comput. Sci.* **2001**, *41*, 1422–1426.